Title

On the performance of a *cointegration*-based approach for novelty detection in realistic fatigue crack growth scenarios

Abstract

Confounding influences, such as operational and environmental variations, represent a limitation to the implementation of Structural Health Monitoring (SHM) systems in real structures, potentially leading to damage misclassifications. In this framework, this study considers *cointegration* as a state of the art method for *data normalisation* in fatigue crack propagation scenarios, where monitoring is performed by a distributed network of strain sensors. Specifically, the work is aimed at demonstrating the effectiveness of cointegration on real engineering data in a new context, where the damage is continuously growing.

Cointegration is applied at first in a controlled scenario consisting of a numerical strain simulation by means of a finite element model, modified in order to take realistic temperature fluctuations and sensor noise into account. Afterwards, detrending and anomaly detection performances are verified in two different experimental programmes on realistic aeronautical structures subjected to fatigue crack growth, including a full-scale fatigue test on a helicopter tail boom. Strain measurements are taken from a network of Fibre Bragg Grating (FBG) sensors, known to be extremely sensitive to temperature variations, hence delivering challenging scenarios for cointegration testing. Results are shown to be in good agreement with the experimental evidence, with the cointegration algorithm capable of detecting the onset of damage propagation within a 4 mm increment from a baseline condition.

Authors

Mauro Salvetti [a], Claudio Sbarufatti [a], Elisabeth Cross [b], Matteo Corbetta [a], Keith Worden [b], Marco Giglio [a]

Affiliations

[a] Politecnico di Milano, Department of Mechanical Engineering, Milano, via La Masa 1, 20156, Italy [b] University of Sheffield, Department of Mechanical Engineering, Mappin Street, Sheffield, S1 3JD, U.K.

Corresponding author

Claudio Sbarufatti: claudio.sbarufatti@polimi.it

Keywords

Fatigue Crack Growth, Cointegration, Fiber Bragg Grating, Strain, Structural Health Monitoring.

1. Introduction

Structural Health Monitoring (SHM) is the engineering discipline concerned with inferring the health and performance of structures on a possibly real-time basis, using networks of permanently installed sensors [1]. There are two main approaches to SHM: model-based and data-based. In the former approach, the analysis is usually founded on a physics-based model e.g. a Finite-Element (FE) model, and then the model is updated periodically in order to track changes in the system parameters that could imply damage; the update algorithm is usually formulated in terms of an inverse problem. In the data-based approach, damage-sensitive features are extracted and machine learning methods are used in order to learn a statistical model

of the data [1]. A problem arises with the data-based approach if one wishes to go beyond damage detection; if it is required to locate or quantify damage, it is necessary to have training data (pre-existing measurements) covering all the damage states of interest. In the case of very expensive or unique structures, it is not usually possible to obtain damage state data, and one relies on *novelty detection*. Novelty detection is a form of *unsupervised learning*, which requires only data from the undamaged (normal) condition of the structure; a statistical model of the undamaged state feature distributions is obtained, and data is subsequently checked for conformity to the normal condition model. Thus, the problem of damage detection is reduced to the problem of *change detection*. Unfortunately, another problem arises then – the problem of *confounding influences*. The features of a structure may change over time for benign reasons, unrelated to damage, and this will commonly occur when structures are operating *in situ*, outside of a controlled environment. The simplest example of this is a bridge; if one were to use natural frequencies as damage-sensitive features for bridge SHM, one would quickly find that the features are also very sensitive to *operational and environmental variations,* which act as confounding influences. For example, the natural frequencies of a bridge will change with temperature, wind conditions and patterns of traffic loading (see [2] for a careful case study). Fortunately, it is possible to remove the effects of confounding influences in various ways; the techniques are collectively known as *data normalisation* methods (a fairly recent survey can be found in [3]).

There are essentially two approaches to data normalisation, depending on whether or not measurements of the confounding variable (e.g. temperature) are available. If measurements of the variable are available, one can use a regression approach to fit the temperature variations and *subtract* them off; in the contrary situation one can identify a subspace of the feature space that traps the variations and then *project* features onto an insensitive orthogonal subspace [4]. A recent development in projection methods for data normalisation, and arguably the current state of the art, is *cointegration* [5-8]. The cointegration methodology originated in the field of econometrics, where it was used in order to categorise and analyse the long-term trending behaviour of multivariate time series; it was introduced for, and adapted, to the problem of data normalisation for SHM in [5,6]. The basic idea is: if a group of time series share a set of common time-varying trends (satisfying certain conditions), there will exist a linear combination of the series purged of the trends; in the context of SHM where long-term trends are usually caused by confounding influences, cointegration removes the influences. Cointegration was also compared to outlier analysis and minor component analysis in [6]. The main limitation of cointegration is that it is a linear theory, restricted to linear combinations of time series, although there have been attempts to develop nonlinear variants for SHM, starting with [9,10]. In an attempt to enhance the sensitivity of damage detection at specific timescales, a multiscale variant of the cointegration algorithm was proposed in [11]. Applications of cointegration in the field of condition monitoring [12,13] and fatigue crack monitoring [14] have recently appeared; in fact, the reference [14] presents a precursor to the current study.

The present study considers the cointegration between signals and the use of the algorithm residuals as an anomaly detector in two test programmes on real aeronautical structures subjected to fatigue degradation and naturally induced temperature variations. The structures involved in the fatigue tests were equipped with Fibre Bragg Grating (FBG) sensor networks for strain recording. Since the type of sensors employed is largely affected by temperature variations, feature extraction from the raw signals cannot be directly performed for the identification of structural anomalies. Although temperature compensation for strain measurements is well established [15], the determination of the set of parameters, needed to establish the compensation, is not straightforward and not always possible, due to temperature gradients along the structure and different structural compliance depending on sensor position. While this can be solved by adopting temperature compensated gauges or by using multiple sensors at each location of interest [16], this becomes impractical when a dense sensor network is required. Hence, the authors aim to demonstrate the effectiveness of cointegration as a promising technique to remove undesirable trends from real engineering FBG strain data, with a view to structural health monitoring. Two studies trying to address anomaly detection insensitive to environmental conditions were published by Yan, Kerschen, De Boe and Golinval [17, 18]. Yan

and co-authors introduced a linear [17] and piecewise linear [18] PCA method to filter out the effect of temperature and perform damage detection on large structures. A major difference between the PCA-based methods and cointegration proposed here is the selection of the number of factors affecting the monitored features required by the former. That may be relatively simple as claimed in [17, 18] when the number of environmental factors is known a-priori. If several unknown factors affect the feature extracted from the signal, the selection of the number of principal components may not be obvious.

Moreover, to.the.authors..knowledge..the.current.literature.on.cointegration, and specifically cointegration-based diagnostic approaches, comprises, almost exclusively, situations where an intact structure experiences a sudden and circumscribed damaging event [3,5-12,19-22]. With such a precondition, the damage onset introduces a change of the system properties, and often results in a clear discontinuity in the recorded sensor data or in the features extracted from such sensor data. Conversely, in the present study a continuous evolution of the damage is taken into account, with the novelty detection algorithm tested in the realistic case of crack growth. In this context, it could happen that training data include the effect of undetected fatigue damages, whose continuous evolution manifests as another long-term trend that could be misinterpreted and removed by cointegration, especially at lower crack lengths. Therefore, the consistency of the detection results is assessed against the inclusion of the phenomenon effects in the training data. In particular, the technique performance is firstly evaluated in a controlled scenario with the aid of an FE model, analysing simulated strain signals. Subsequently the potential of the implemented algorithm is verified on three different experimental cases including metallic stiffened panels representative of a helicopter rear fuselage and a full-scale helicopter tail boom.

The layout of the present article is organised as follows. First, an introduction to the mathematical formulation of the method is presented in Section 2. After this, the details of the experimental tests are given and the effect of environmental variations is explained and shown in Section 3. In Section 4, the numerical activity is presented, and an assessment on the performances of the cointegration algorithm on simulated data is provided in Section 5. Finally, in Section 0, the algorithm is tested on the experimental data, recorded by the FBG sensors positioned on the structures, and.performances.on.a..real-scenario..are.evaluated.

2. On the application of cointegration to engineering data

In order to make the paper more self-contained, a brief introduction to the cointegration methods will be given, closely modelled on [4].

Cointegration is a property of multiple nonstationary time series [5,23,24]. Two or more nonstationary time series are said to be *cointegrated* if some linear combination of them is stationary. Mathematically, a multivariate nonstationary time series $\underline{y_i}$ is cointegrated if a vector $\underline{\beta}$ exists such that z_i is stationary, where,

$$z_i = \underline{\beta}^T \underline{y_i} \tag{1}$$

If this condition holds, $\underline{\beta}$ is termed a *cointegrating vector*. In general, there may be multiple cointegrating vectors; in fact, if $\underline{y_i}$ is *n*-dimensional, there may be up to *n-1* linearly independent cointegrating vectors. A more precise definition of cointegration requires one to introduce the concept of an *order of integration*; this is the number of times one must difference a nonstationary time series before it becomes stationary. For engineering applications, most variables of interest can be considered to be integrated of order 1 (denoted $I(1)$), which implies that their first differences will be stationary [19]. In general, a set of time series are cointegrated if they share a common order of integration and a linear combination of the variables exists with a lower order of integration. The first step in cointegration analysis is usually to ascertain the order of integration of each of the variables to be included in the analysis. This assessment is commonly achieved in econometrics by testing each variable for a *unit root*; if a unit root is present in the characteristic equation that defines some time series, then that time series will be inherently nonstationary. The unit root test

discussed briefly and used here is called the *Augmented Dickey Fuller* (ADF) test; readers should refer to [25,26] or [3] for more details and background theory. The ADF test involves fitting each variable to a model of the following form,

$$\Delta y_i = \rho y_{i-1} + \sum_{j=1}^{p-1} b_j \Delta y_{i-j} + \epsilon_i \tag{2}$$

where the difference operator Δ is defined by $\Delta y_{i-j} = y_{i-j} - y_{i-j-1}$. A suitable number of lags p need to be included to ensure that the residual sequence ϵ_i becomes a white noise process [23]. This equation is an example of an *error correction model* (ECM). In this form, the stability (and therefore stationarity) of the model in equation (2) is determined by the value of ρ; if it is statistically close to zero the process will be nonstationary and integrated of order one, $I(1)$. The idea of the ADF statistic is therefore to test the null hypothesis of $\rho = 0$, by comparing the test statistic,

$$t_\rho = \frac{\hat{\rho}}{\sigma_\rho} \tag{3}$$

where $\hat{\rho}$ is the least-squares estimate of ρ and σ_ρ is the variance of the estimate, against critical values that can be found in [27], in much the same way that one would when conducting a Student's *t*-test. The hypothesis is rejected at level α if $t_\rho < t_\alpha$. If the hypothesis is accepted, the time series has a unit root and is $I(1)$. If the hypothesis is rejected, the test should be repeated for Δy_i ; if the hypothesis is then accepted y_i is an $I(2)$ nonstationary sequence. This is continued until the integrated order of the time series is found. Additional hypotheses tests are needed if the model form is extended to include shifts or deterministic trends (or both) [25,26]. Once the order of integration of each of the variables of interest has been determined, those that are integrated of the same order can then be included in a cointegration analysis.

One of the most common approaches to finding cointegrating vectors is the Johansen procedure [28]; this is based on finding the 'most stationary' linear combination possible for a set of nonstationary variables. This procedure is most often used with $I(1)$ variables and is based on a maximum likelihood argument. The theory is complex and will not be included here (the interested reader can consult [23,28]); however, as before, the necessary steps to implement the Johansen procedure will be provided without justification. The first step of the Johansen procedure is to fit the variables in question to a Vector AutoRegressive (VAR) model of order p (where the order is determined in some principled manner), which is then converted into a *Vector Error Correction* (VECM) model of the form,

$$\underline{z}_{0i} = AB^T \underline{z}_{1i} + \Psi \underline{z}_{2i} + \underline{\epsilon}_i \tag{4}$$

where $\underline{z}_{0i} = \Delta \underline{y}_i$, $\underline{z}_{1i} = \underline{y}_{i-1}$ and $\underline{z}_{2i} = (\Delta \underline{y}_{i-1}, \Delta \underline{y}_{i-2}, \cdots, \Delta \underline{y}_{i-p})^T$. The most stationary linear combinations of the variables, or cointegrating vectors, are to be found in the matrix B in the VECM. However, the VECM cannot directly be found via standard least-squares methods as it represents a rank-deficient system; instead, one proceeds to estimate B via the residuals of two other regressions,

$$\begin{aligned} \underline{z}_{0i} &= C_0 \underline{z}_{2i} + \underline{R}_{0i} \\ \underline{z}_{1i} &= C_1 \underline{z}_{2i} + \underline{R}_{1i} \end{aligned} \tag{5}$$

From these residuals, the following product moment matrices can be defined,

$$S_{mn} = \frac{1}{N} \sum_{i=1}^{N} \underline{R}_{mi} \underline{R}_{ni}^T \qquad m, n = 0,1 \tag{6}$$

Finally, using the moment matrices, the cointegrating vectors are found as the eigenvectors of the generalised eigenvalue problem,

$$(\lambda_i S_{11} - S_{10} S_{11}^{-1} S_{10}) \underline{v}_i = \tag{7}$$

The cointegrating vector that will result in the most stationary combination of the original variables will be the eigenvector $\underline{v}_i$ corresponding to the largest eigenvalue λ_i. If the eigenvectors are assembled columnwise into a matrix, the result is the matrix B for the VECM of equation (4). Again, readers are referred to [5,23,24] for more details of the theory.

From a practical SHM point of view, the cointegrating vectors of a set of variables should be established using data from some training period from the undamaged structure that encompasses the full range of the anticipated environmental and operational variations, manifesting as linear long-term trends. Upon projecting new data onto a cointegrating vector, the combination will remain stationary all the time the structure continues to act in its normal condition, but should become nonstationary on the introduction of damage, which also manifests as long-term trends, but different from those associated with temperature and often non-linearly. Cointegration projects out components of data that correspond to the linear long-term trends seen during training, i.e. which create nonstationarity. This makes cointegration a promising solution for anomaly detection in the presence of unexpected trends among engineering time series, such as those related to temperature-induced strains on FBG sensor readings.
As anticipated, in this paper the inclusion of data from a damage scenario in the cointegration training set is also considered. Of particular interest is the behaviour of the cointegrated residual when some crack growth has occurred in the training duration. It is anticipated that the cointegrating vector will capture and repress a linear component of the relationship between strains induced by crack growth, but that damage sensitivity will remain owing to nonlinear effects. In the following sections, simulated and experimental data will be used to explore this.

3. Experimental activities and acquired data

As described in the introduction, two main experimental activities are considered in this study. Specifically, the first comprises fatigue crack growth (FCG) tests on aeronautical aluminium panels; the second is a full-scale FCG on a helicopter tail-boom. In both cases, optical FBG sensors are used for strain measurement, leveraging on their exceptional advantages like low power consumption, light weight, immunity to electromagnetic interference, long lifetime and high sensitivity, however recognising that they are very sensitive to temperature fluctuations.

FBGs make use of a periodic modulation of the refractive index that can be photo-written in an optical fibre core. When the light passes through the optical fibre, the Bragg grating reflects a specific wavelength λ back, which changes if a local deformation is present due to mechanical loads or temperature. The relationship between mechanical strain, temperature and central wavelength of the reflected light spectrum can be expressed as,

$$\frac{\Delta\lambda}{\lambda_0} = \frac{\lambda - \lambda_0}{\lambda_0} = k\left(\varepsilon_m + \alpha_{sp}\Delta T\right) + \alpha_\delta \Delta T. \tag{8}$$

Where λ is the reflected wavelength in the deformed condition, λ_0 is the reference wavelength, k is the gauge factor, α_{sp} is the expansion coefficient of the specimen material, α_δ is the change of refraction index per unit temperature, and ΔT is the temperature variation. Indeed, the total measure is the sum of the strain caused by mechanical loads ε_m, that caused by thermal variations $\alpha_{sp}\Delta T$ and the apparent strain caused by modification of the refraction index $\alpha_\delta \Delta T$. When damage propagation monitoring is the objective, the temperature effect must be compensated for, as it could hamper the damage identification process if its effect is comparable or even higher than the sensitivity to damage. However, the temperature field is usually not uniform on the monitored structure, thus requiring multiple thermal measures for a correct and effective compensation. Moreover, even assuming a uniform thermal field, strains induced by thermal gradients strictly depend on the boundary conditions, i.e. the compliance of the measured area, especially for overconstrained structures. These aspects require, for an ideal compensation of the thermal effect, the strain

to be measured from a second, identical structure undergoing the same temperature field, measured on the same locations, but mechanically unloaded. Obviously, such a solution is not realistically feasible and only remains a valid possibility for small-scale laboratory tests. Although other solutions are readily available commercially, including different means of temperature compensation on foil gauges and a variety of commercial temperature-compensated gauges [16], their dimensions is not often compatible with the deployment of a dense sensor network. In this framework, cointegration can have a clear advantage. Indeed, assuming that the temperature variation would introduce common trends within the measured signals, cointegration would automatically remove such a temperature effect, with the residuals highlighting the presence of anomalies in the recorded signals, *i.e.* potential damages in the structure, without any *a-priori* compensation.

3.1.Aluminium panels test set-up

The tested aluminium panels, displayed in Fig. 1, replicate the actual rear fuselage components of a medium-heavy weight helicopter. Additional reinforcements were added to the specimens, especially near the constrained zones, in order to obtain a stress field congruent with the real working condition on the rotorcraft. Dimensionally, the panel has a 500x600 mm skin with four riveted vertical stringers of length 435 mm. The skin is made in Al2024-T6, while the stringer and the additional reinforcements are in Al7075-T76.

For the first specimen – hereafter, denoted *Panel-SC* – an artificial notch was created in a central position on the skin bay. This artificial defect can be considered representative of a generic impact damage, causing nucleation of a Skin Crack (SC). The second sample – *Panel-RC* – had a rivet removed and then, as before, a crack was propagated from an artificial defect located into the panel skin. Rivet-propagating Cracks (RC) can occur in this kind of rotorcraft structure, as rivet holes can act as stress concentrators. Locations of the artificial notches are shown again in Fig. 1. In both cases, after creation of the artificial notch, a certain number of load cycles was required for the nucleation of an actual crack from the artificial notches. A steady condition is expected on the measured strain signals before crack propagation, hereafter referred to as baseline.

The optical fibre carrying the FBG sensor network was bonded to the structure onto the four stringers with a two-component adhesive, including a total number of 20 FBG sensors. Specifically, the sensors are FBGS Draw Tower Gratings (DTG®s) written in Low Bend Loss fibre LBL-1550-125. Each grating is 8mm long and they are positioned close to the stringer edge, with a gap of 60mm between one another. The locations of the gratings, between two consecutive rivets, are highlighted in Fig. 1. An additional FBG is used for temperature measurement; however, its data are not considered in this study for temperature compensation, which is only achieved by the cointegration-based technique.

A cyclic fatigue load was supplied by a hydraulic actuator, and the specimen fixture apparatus assured that the load was applied only in the vertical direction. In particular, the load cycle was a sinusoidal function with a frequency of 12 Hz and a load ratio R, defined as the ratio between the minimum and the maximum values within one load cycle, equal to 0.1 for both test cases. For Panel-SC, the peak load was kept constant at 35 kN, while for Panel-RC three different operational conditions were imposed with the peak force reaching 35 kN for the first $\times$ ^{5} cycles, than 25 kN for about $\times$ ^{5} cycles and finally the test was concluded at 30 kN of peak force. Again, a certain number of load cycles is needed in order for the crack to start propagating, and a portion of those load cycles has been used here as a baseline. Although the fatigue tests were stopped at predefined intervals for visual inspection and crack length measured by a caliper, the exact instant of crack nucleation was not identified, thus posing additional uncertainty in the identification of the baseline limits for cointegration algorithm training.

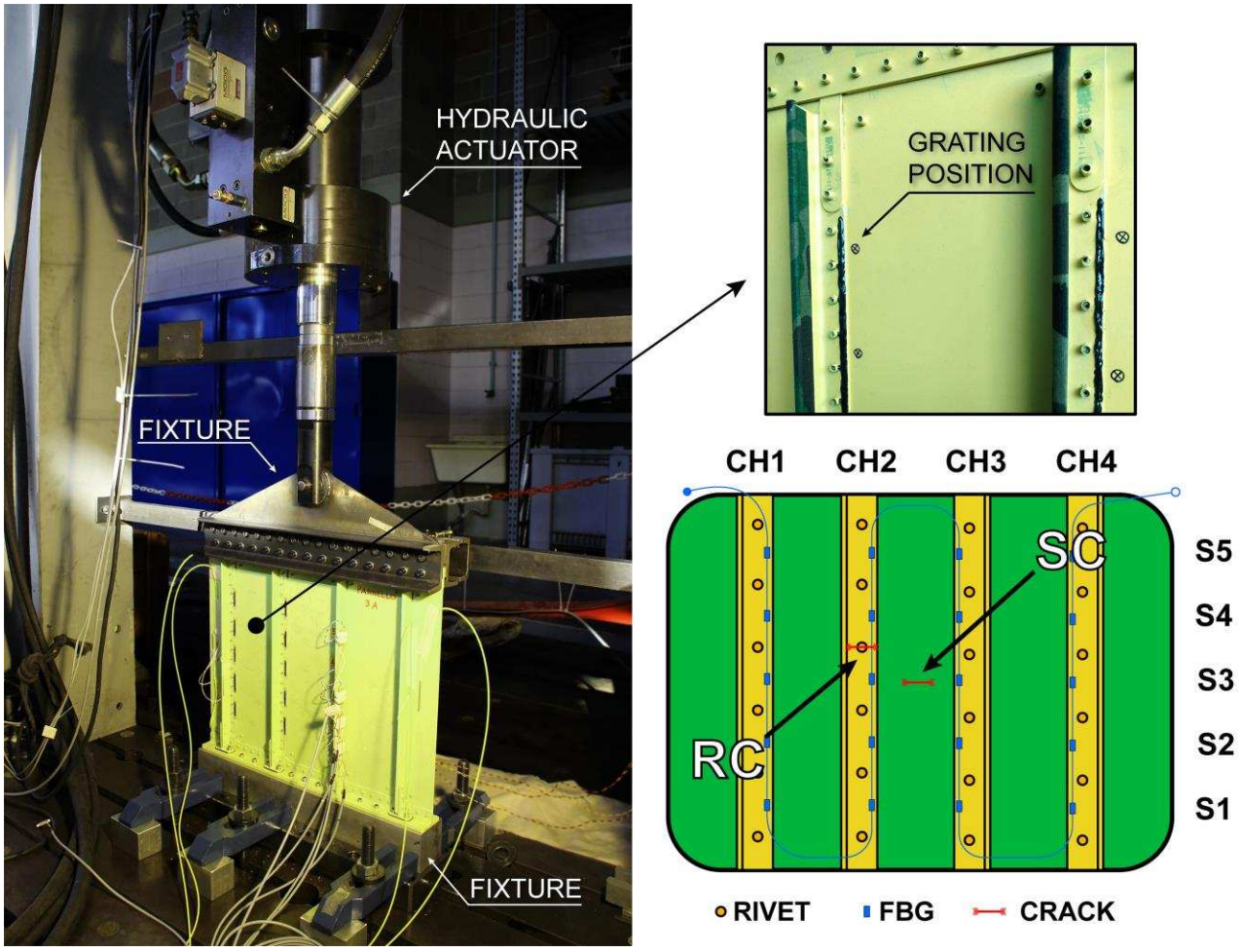

Fig. 1: Experimental test configuration for the aeronautical panels, on the left, and location of FBG sensors and cracks (rivet crack, RC, and skin crack, SC) on the right.

3.2.Tail boom test set-up

The second FCG test activity was performed on the tail boom of a retired Military Mi-8/17 helicopter provided by the Air Force Institute of Technology of Poland. As shown in Fig. 2, the tip of the tail carrying the tail rotor was removed, while the root of the tail was connected to a rigid frame by means of a dedicated structure in CFRP material. This constraint was calibrated on the stiffness of the rotorcraft central fuselage, thus reproducing realistic boundary conditions. The fatigue load was applied on the free end, transversally to the tail axis, to simulate the effect of the tail rotor and to induce bending and torsion at the root of the tail. Specifically, the applied load was again of a sinusoidal form with frequency 1.5 Hz, peak value 8 kN and load ratio R=0.1.

A series of optical fibre sensors were mounted on the inside stringers of the structure. In particular, nine FBGs were positioned on five stringers, for a total of 45 sensors, as shown by the schematics in Fig. 2. The same type of sensors as for the panel structures is considered here. The crack was artificially initiated at a rivet hole (after rivet removal) by inserting a notch approximately 15 mm-long, specifically on stringer STR7, between sensors S5 and S6. Two crack gauges were also applied to monitor the crack growth. The ambient and structure temperatures were also measured by a thermometer and a dedicated FBG sensor. However, as previously stated, the data from the two instruments will not be used here to compensate the temperature-effect on the strain signals.

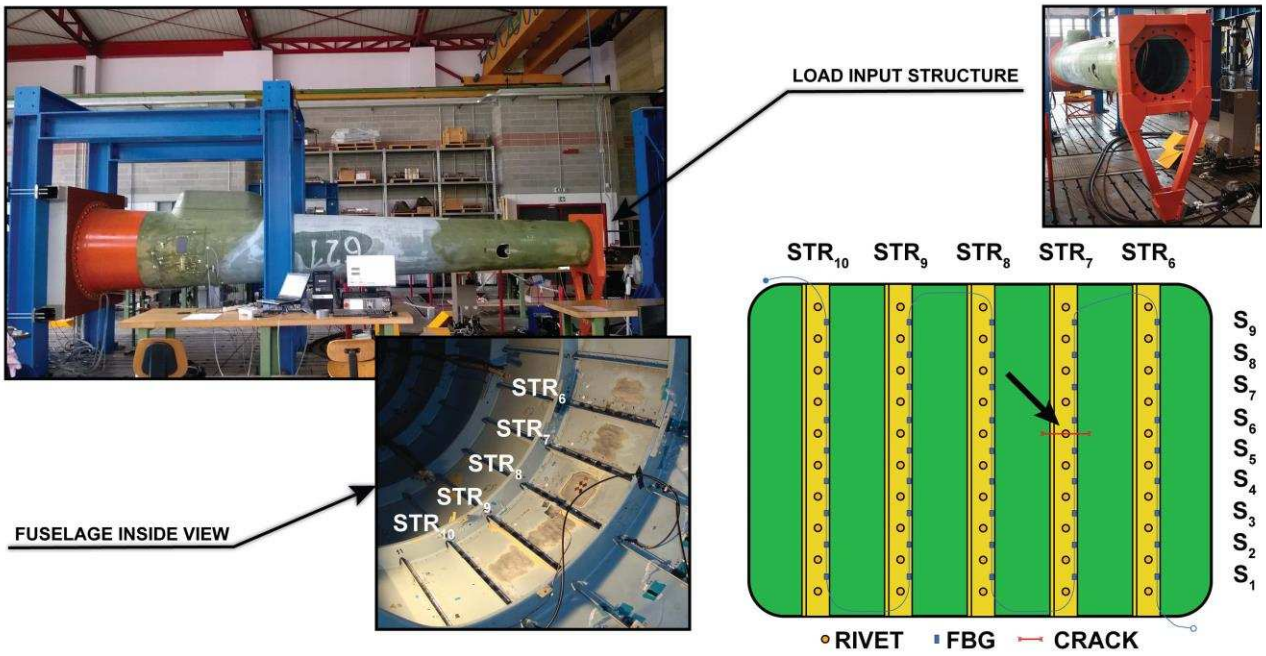

Fig. 2: Experimental test configuration of the Mi-8 helicopter tail boom (a) and location of the crack monitored during the FCG tests.

3.3.Signal acquisition and temperature effect

For both the experimental activities, the FBG signals were acquired with a HBM-DI410 dynamic interrogator with four channels and a maximum sampling frequency of 1 kHz. In order to reduce the data size, only a specific number of cycles were recorded during the fatigue tests: in particular, 30 cycles every 500 cycles of the fatigue test were acquired, with the maximum sampling frequency allowed by the system. In post-processing, as shown in Fig. 3a, the wavelength peak shifts, caused by the sinusoidal load, were extracted from these blocks of data. The average peak level of the data block was then stored to create the time series of strain values for each sensor.

An example of the strain signals recorded from the first stringer sensors from the Mi-8/17 tail test is shown in Fig. 3b, highlighting the problem previously discussed in Section 2. In particular, the first ^{5} cycles are displayed, during which the crack had not started its propagation yet, however showing a 200 με. strain. variation solely due to the temperature shift, *i.e.* to the sun gradually hitting the tail boom as the day went on (at $\times$ ^{4} cycles the test was stopped and then resumed the next day). This strain trend induced by thermal effects can easily hide the crack-induced change of the structure behaviour, especially at the early stages of propagation. Thus, a compensation for this effect is needed to isolate the damage-induced strain deviations from a generic baseline condition.

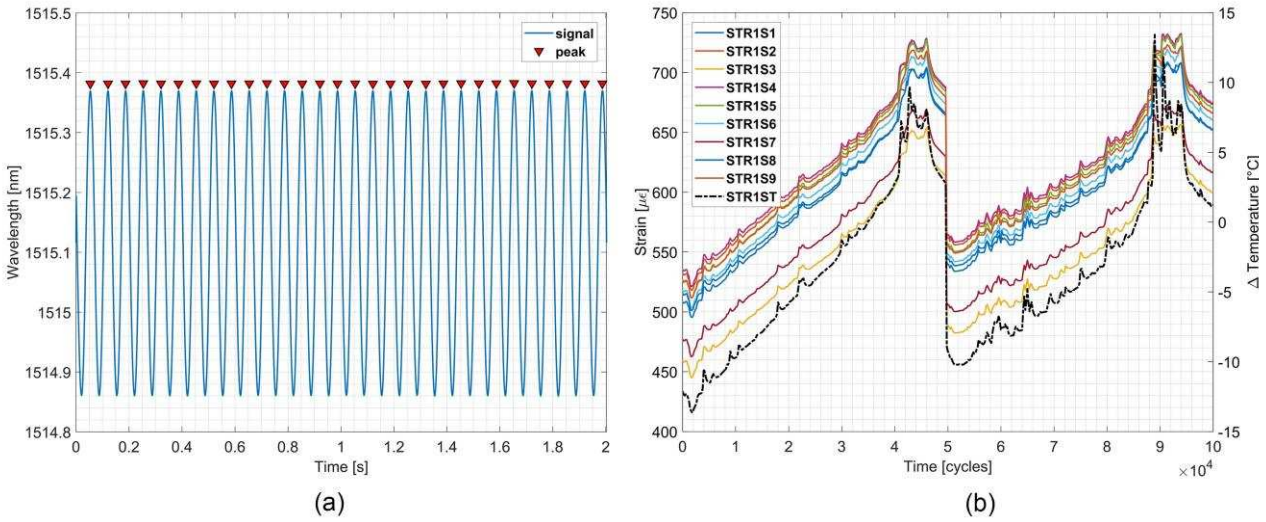

Fig. 3: Example of the acquired FBG signals with highlighted peaks (a) and variation of mean value of the strain peaks (b) due to temperature shift (black dash-dot line, measured by the dedicated FBG sensor).

4. Simulating thermal effects on measured strain

In order to get an understanding of the different contributions on the strain field, FEM simulations of the aluminium panel shown in Section 3.1 were carried out in Abaqus® 6.14-5. The simulated strain signals were generated not only taking the effect of crack propagation into account but also the influence of thermal expansion. The FEM model is shown in Fig. 4, with a rivet crack (Panel-RC) highlighted by the stress contour plot. Rivets were modelled as springs with proper stiffness values in the three directions, connecting the components of the panel. Specifically, the springs/dashpots feature was used, defining for each rivet point three connection interactions between the skin panel and the stringers: each interaction refers to one of the three degrees of freedom, of which the appropriate stiffness was analytically derived. Boundary conditions were opportunely chosen to replicate the structure fixture of Fig. 1.

Several simulations were carried out with semi-crack lengths ranging from 2 mm to 25 mm, and for a static load of 35 kN applied vertically as for the peak load condition of the real experimental test. The same simulations were subsequently repeated with a thermal field, constant through the thickness of all the different panel components (skin, stringers, reinforcement plates, etc.). Specifically, a 10°C increment in temperature was considered. Finally, the strain values along the stringer axis (E22) were extracted at coordinates coincident with the sensor positions of the real panels. In Fig. 5, the obtained database of simulated strain values, as a function of the semi-crack length, is shown for the two thermal conditions (0°C and 10°C). The progressive strain increase caused by the crack propagation is easily recorded by sensor 3 on channel 2, the closest sensor to the crack, in both cases. A noticeable raise of the overall strain pattern is observed when the thermal field is applied to the panel.

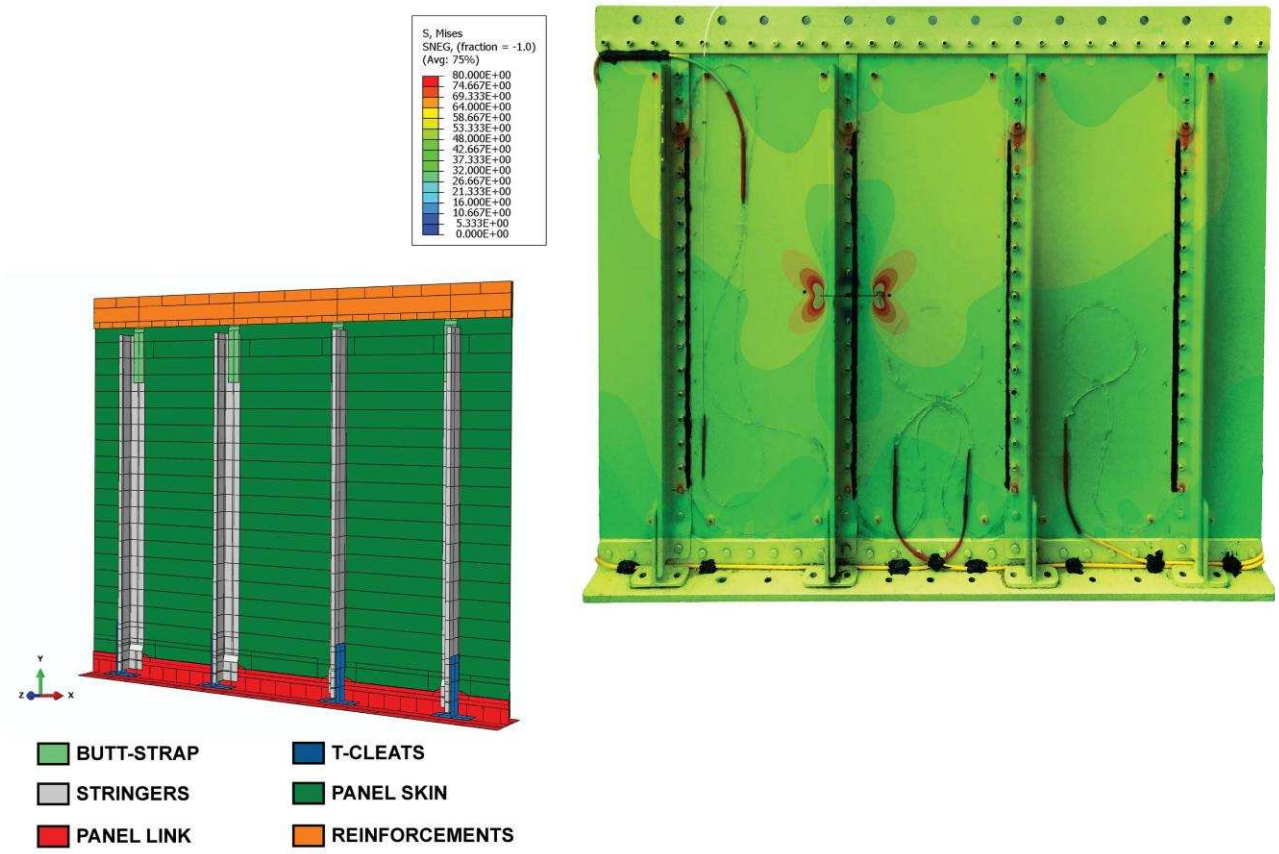

Fig. 4: FEM model (right) with highlighted components and Panel-RC with superimposed stress contour plot.

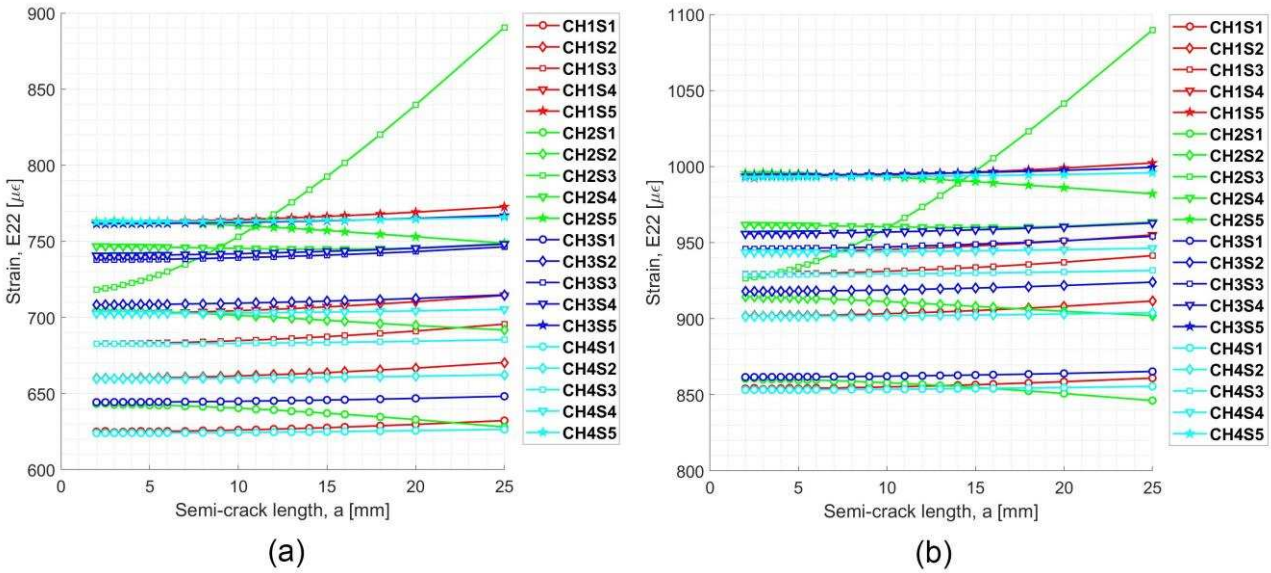

Fig. 5: Strain values (E22 component, vertical direction) of the 20 simulated sensors for the case without (a) and with (b) thermal field.

4.1.Linking the strain value with time

Since the objective is to analyse a time series, the strain value must be linked to a time step. To do so, the Paris law for crack propagation [29] is taken into account: for every semi-crack length a, the number of cycles needed for its propagation can be calculated. Specifically, with C and m as Paris coefficients, stress ratio R, and Walker parameter γ, to account for $R >$, the speed at which the crack grows is given by,

$$\frac{da}{dN} = \frac{C\Delta K^m}{(1-R)^{m(1-\gamma)}} \tag{9}$$

where the stress intensity factor range is

$$\Delta K = \beta(a)\Delta\sigma\sqrt{\pi a} \tag{10}$$

with $\beta(a)$ the geometry factor, a function of the semi-crack length expressed as in [30] for stiffened plate structures, and with $\Delta\sigma$ the far-field stress range applied to the structure. Once the previous parameters in relation to the material of the specimen and to the characteristic of the loading considered were defined, a Matlab iterative routine was implemented. At every k step, if a finite $\Delta a_k = a_k - a_{k-1}$ is imposed, the related variation of the stress intensity factor ΔK_k can be calculated. Thus, the propagation speed of Eq. 9 is known and the ΔN_k cycles needed for that Δa_k can be found.

The database previously created comprises only 22 semi-crack lengths. The calculation of the N cycles, at which those lengths will be reached, is carried out on a higher sampled semi-crack vector, in order to avoid biases in the numerical integration of the.Paris.s.law. The related strain values are consequently interpolated over the new crack step with a piecewise cubic polynomial to preserve the function shapes of Fig. 5. The obtained strain-cycle function is show in Fig. 6a for the first temperature condition. Again, in order to have more samples and an evenly spaced vector, the obtained strain-cycles function is resampled/interpolated over a new time vector with higher resolution.

4.2.Temperature and noise

Based on the compensator FBG used during the fatigue test of the Panel-RC, a temperature signal is extracted, smoothed and resampled to match the resolution of the simulated signals. The temperature trend of Fig. 6b comprises full day transitions and is used to linearly interpolate between the two strain signals databases of Fig. 5 (plus 0°C and plus 10°C) at every time increment. Moreover, uncorrelated Gaussian noise is added to the simulated signals. In fact, noise is always present in reality to some degree and, in the simulation, it also improves the conditioning of the linear algebra needed for cointegration. Specifically, the additive noise has a standard deviation of 0.25 με, selected by analysing the real FBG signals. Eventually, a baseline was also added, with the initial data only influenced by the temperature field variations, before enabling the start of crack propagation at ^{6} cycles. The simulated, but realistic, final signals are shown in Fig. 7.

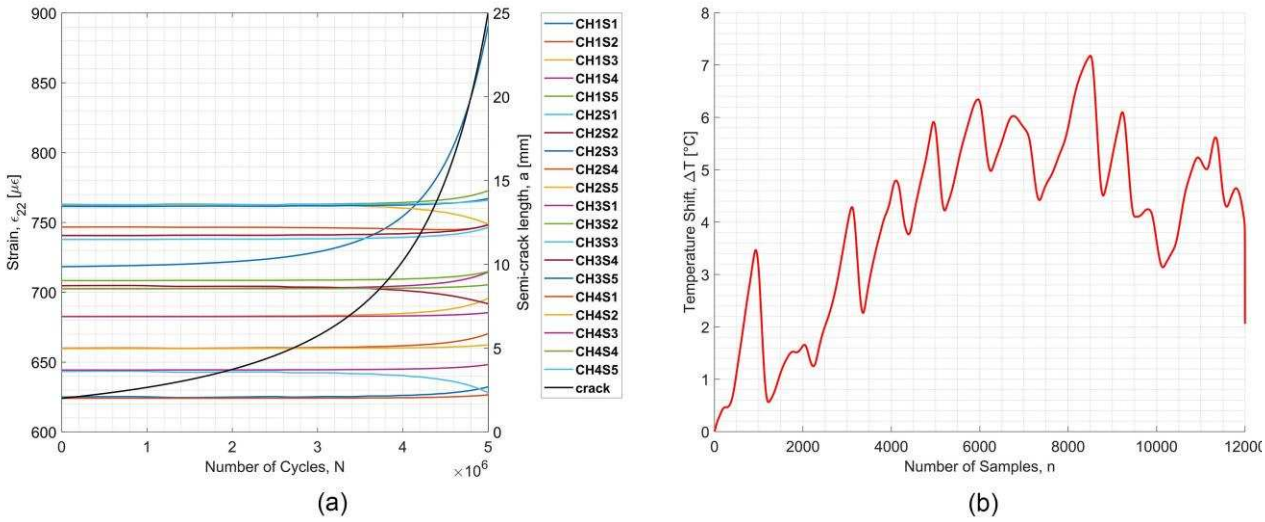

Fig. 6: Simulated strain signals and crack length history (a) and temperature signal from the compensator sensor (resampled and smoothed).

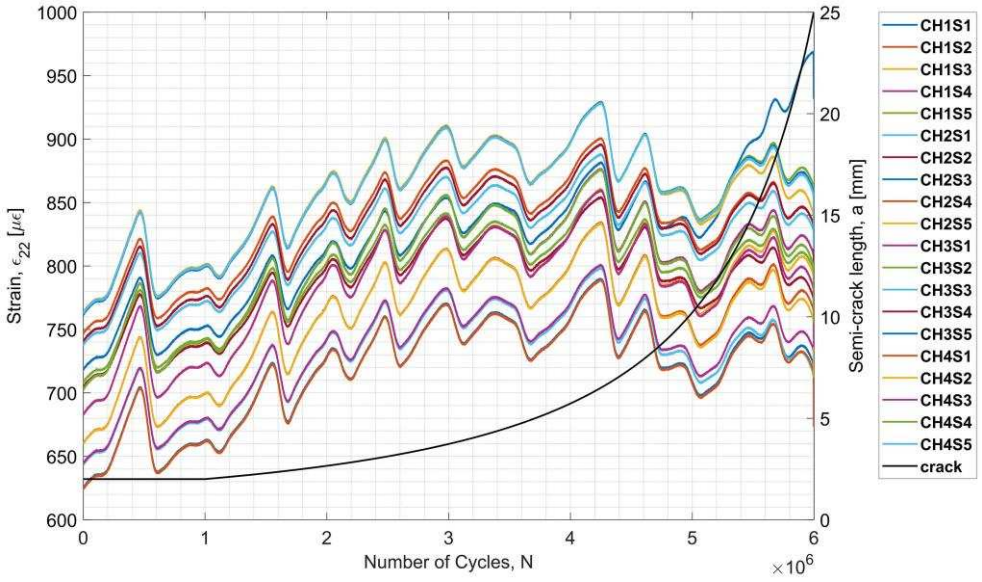

Fig. 7: Simulated strain signals at a constant 35kN reference load, with superimposed temperature effect, and crack length history.

5. Cointegration performance assessment on numerically-simulated strain field

The cointegration method described in Section 2 is applied here to the simulated strain signal described in the previous section. The objective here is to detect an anomalous deviation of the cointegration residuals (i.e. the detrended time series obtained by projection onto the cointegrating vector) in a controlled scenario, specifically analysing how the temperature induced correlation between strain signals is ruined during damage extension and verifying the algorithm response on the introduction of damage sensitive data in the training. Part of the strain time series data are used as training datasets and each series is tested for a unit root process with the ADF test prior to the application of the Johansen procedure. The obtained cointegration

residuals are subsequently tested for stationarity, *i.e.* reliability of the obtained monitoring feature: the ADF test is again used, seeking the rejection of the null hypothesis [25,26].

The 20 simulated signals, each one normalised by its mean and standard deviation for an easier interpretation of the trends, and the residuals of the cointegration, performed considering all the 20 simulated signals, are shown in Fig. 8. The 'novelty detection' (the red circle) refers to the moving average of the residuals exceeding the $\pm 2\sigma$ confidence band, where σ is the standard deviation of the cointegration residuals of the training set. The confidence band acts as a statistical process control X-chart [31], so that if subsequent strain measurements leave the control interval, an anomaly in the structure behaviour can be assumed to exist. Taking the moving average as the monitoring feature has the advantage of avoiding false alarms caused by transient spikes of the residuals due to any potential discontinuities in the data. However, it should be noted that the choices of the moving average window length, the end-point of the training set and the detection strategy could have an effect on the detection time instant. In the specific case of Fig. 8, with a training set including the 'baseline' up to 8×10^5 cycles (vertical black solid line), the cointegration residuals are seen to leave their stationary behaviour at about 2.1×10^6 cycles with an increment of the total crack length of 1.4 mm.

Here, the moving average appeared as a good choice to filter the residual trend, even if the selection of an excessive window length may add some delay to the novelty detection instant. However, more advanced approaches may be adopted to detect when (or if) cointegrating residuals are no longer stationary, or if they no longer belong to a Gaussian distribution, reducing the effect of heuristic choices on the final algorithm performance.

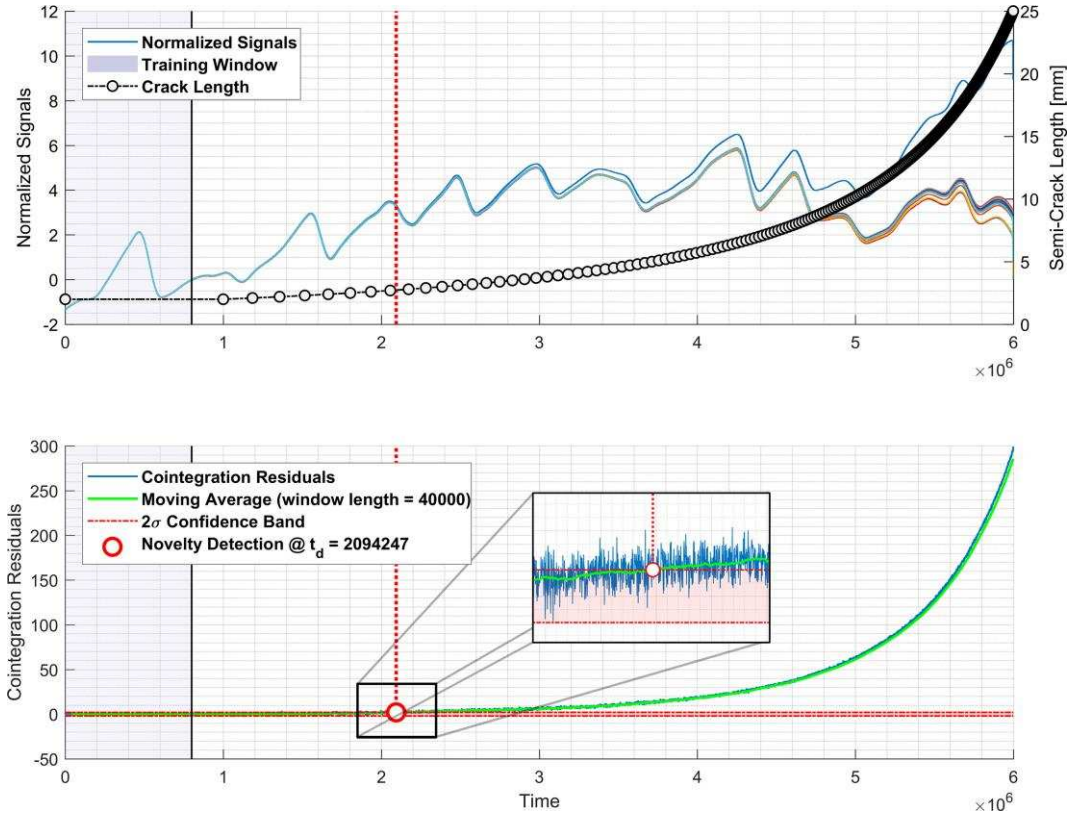

Fig. 8: Cointegration of FEM signals - all sensors are considered. In the upper plot, normalised signals (coloured) are displayed along with the crack length (black circled points) as a function of time (number of cycles). In the lower plot, the cointegration residuals are shown, with a focus of the instant when the moving average (green line) of the residuals (blue line) leaves the confidence band (in red). The training data window is highlighted in grey in both plots.

Furthermore, the selection of the training set length is non-trivial, and varies with data availability and with the fact that, in some cases, the true health condition of the structure is unknown, potentially causing the inclusion of undetected damage condition in the training domain. The latter can be a common situation with large structures like bridges, high-rise buildings, or large airframes when subject to ageing. In our applications, the algorithm designer may wonder whether the training set includes part of data relative to the initial crack propagation. This is a very important point. The cointegration algorithm is actually able to remove (project out) multiple trends. If a period of crack growth is included in the training data, it is possible that the cointegration algorithm will identify the damage progression simply as another trend, potentially removing it. However, one can argue that, if a small portion of data from initial crack progression is included in the training data, cointegration will not project out all evidence of crack growth. According to the Paris law, the crack will propagate at an exponential rate; however, assuming that only incipient crack growth is present in the training data, and bearing in mind the highly local nature of strain sensors, the effects of the crack in the different sensor signals will manifest as strain trends approximated by low-order monomials of different powers. The cointegration algorithm will effectively linearise the trends in order to remove them. However, any further crack growth not included in the training dataset would require a new cointegrating vector for trend removal. Thus, even if a small portion of crack growth is present in the training data, the algorithm will still detect it once the nature of the cointegration relation changes due to crack progression.

To better understand what may happen when damage data is included in the cointegration-training period, Fig. 9 shows the relationship between two of the simulated strain measurements, close to and far from the crack respectively, with the colour of the line representing the length of the crack at that instant. The reader should note that this does not provide a complete picture of the behaviour of the residual, as this is comprised of multiple measurements and not just the two measurements shown. However, studying Fig. 9, one can see that as the crack grows, the relationship between the strain measurements evolves, which is why cointegration is able to detect it. Interestingly, the evolution appears to manifest itself as linear relationships with changing gradients until the crack dimension becomes significant. If the training period were increased to include data from one of these regimes, the sensitivity of the residuals to crack growth would not reassert itself until the gradient of the linear relationship changed sufficiently.

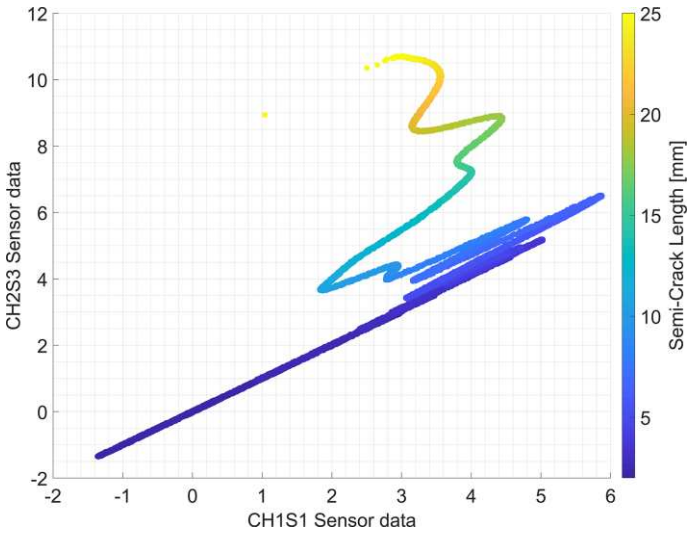

Fig. 9: Correlation plot between two of the FEM-generated signals, one from a virtual sensor close to the crack (CH2S3) and one relatively away from it (CH1S1). The different data points are coloured accordingly to the corresponding semi-crack length value.

In order to evaluate the performance of the algorithm when different crack lengths are included into the training, increasing training set lengths are considered starting from 10% up to 80% of the entire time series. In Fig. 10a and 10b, the results of this sensitivity assessment is shown in terms of novelty detection time as a function both of size of the training dataset and the maximum length of the crack that the training dataset

includes. When most of the training set is associated to the baseline condition (non-propagating damage), the detection happens quite early after only a few millimetres of crack evolution. As the training data includes more of the crack propagation, the anomaly is identified later and later until reaching a plateau around 5.5×10^6 cycles. Thus if the calculation of the cointegrating vector is based on data that contain little of the investigated phenomenon, as discussed above, the appearance of contributions of higher order can still trigger the detection. On the contrary, once the crack growth is mostly included in the training dataset, only steep changes in propagation speed are detected, as after the 5.5×10^6 cycles in this case.

It is finally worth noticing that, provided the cointegrating vector projects out the environmental influences included in the training, the resulting residuals can be expected to replicate the effect of crack length on the strain signals. This is confirmed in Fig. 11, where the non-linear correlation between cointegration residuals and crack length is evident, with non-linearity related to the non-linear dependence of the strain measures from the crack length. Although outside the scopes of the present study, this information can be exploited in future activities in the context of damage prognosis.

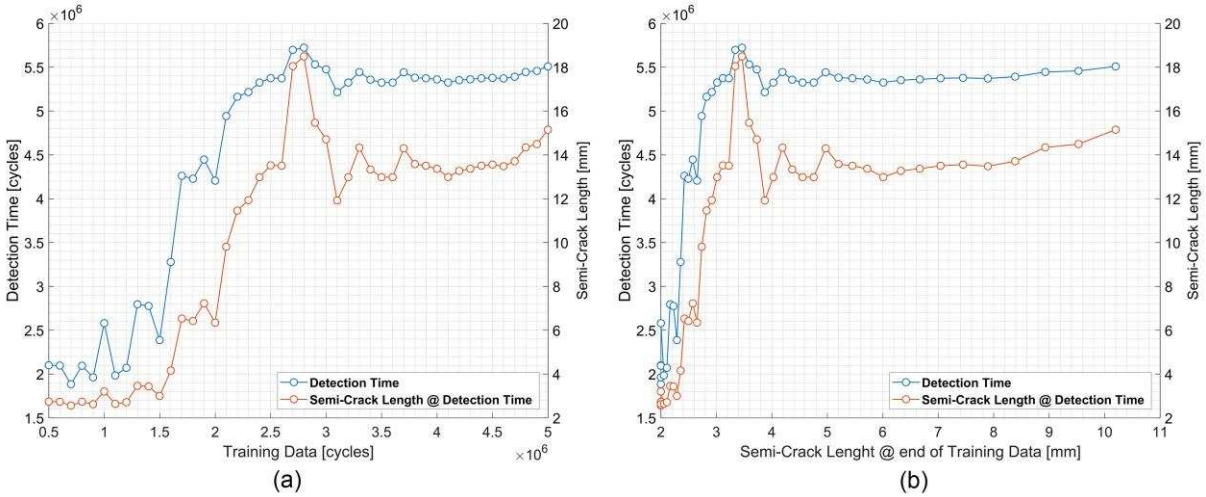

Fig. 10: Detection time and crack length at detection as a function of number of cycles considered as training data (a) and as a function of the crack length at the end of the considered training data (b).

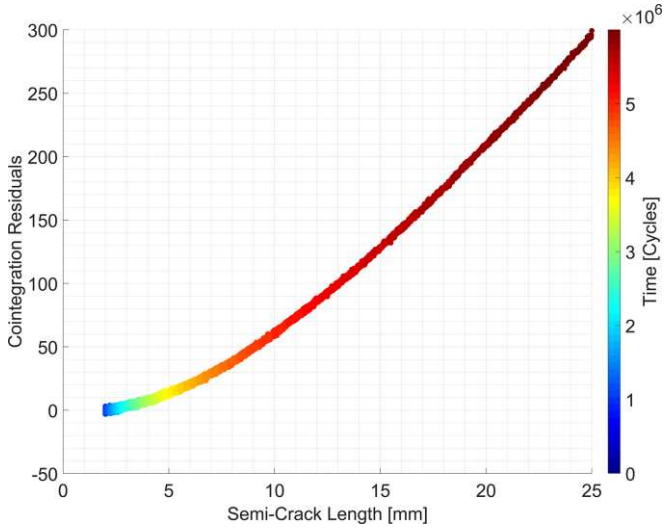

Fig. 11: Correlation plot between the cointegration residuals and the crack length trend for the simulated panel case. The data points colour indicates time.

6. Application to experimental data

The cointegration algorithm is now applied on the experimental data introduced in Section 3.

6.1.Fatigue crack growth detection in Panel-SC

The normalised signals acquired during the test of Panel-SC are displayed in Fig. 12. As highlighted, the test was paused at around . × ^{5} cycles and then resumed the same day. During the first half of the test, a cyclic variation of the strain is present due to temperature oscillations in the laboratory. As before, part of the baseline is used for training, or for the evaluation of the cointegrating vector. The cointegration residuals maintain their stationarity inside the baseline, and then begin to deviate after an increase of the total crack length of less than 3 mm. Moreover, the test pause does not affect the cointegration residuals (or at least only marginally) since no changes were produced on the structure between one and the subsequent part of the experiment and the temperature is assumed to have ranged similarly. The abrupt rises of the residuals at . × ^{5} and at . × ^{5} cycles are due to significant changes in boundary conditions: indeed, the test was suspended again but this time also the panel itself had to be removed and then reinstalled for logistic reasons.

In Fig. 13, regarding the correlation between two sensors, one close and one far from the damage, a similar behaviour can be noticed as expected from the previous simulation. In particular, the effect of the crack in a stiffened panel can be assumed to be localized as well as the measure from an FBG, due to its own dimensions. These characteristics of the system justify the fact that only when the crack reaches a size that cannot.be..ignored. by the stiffened structure, the gradient of the linear relationship changes significantly.

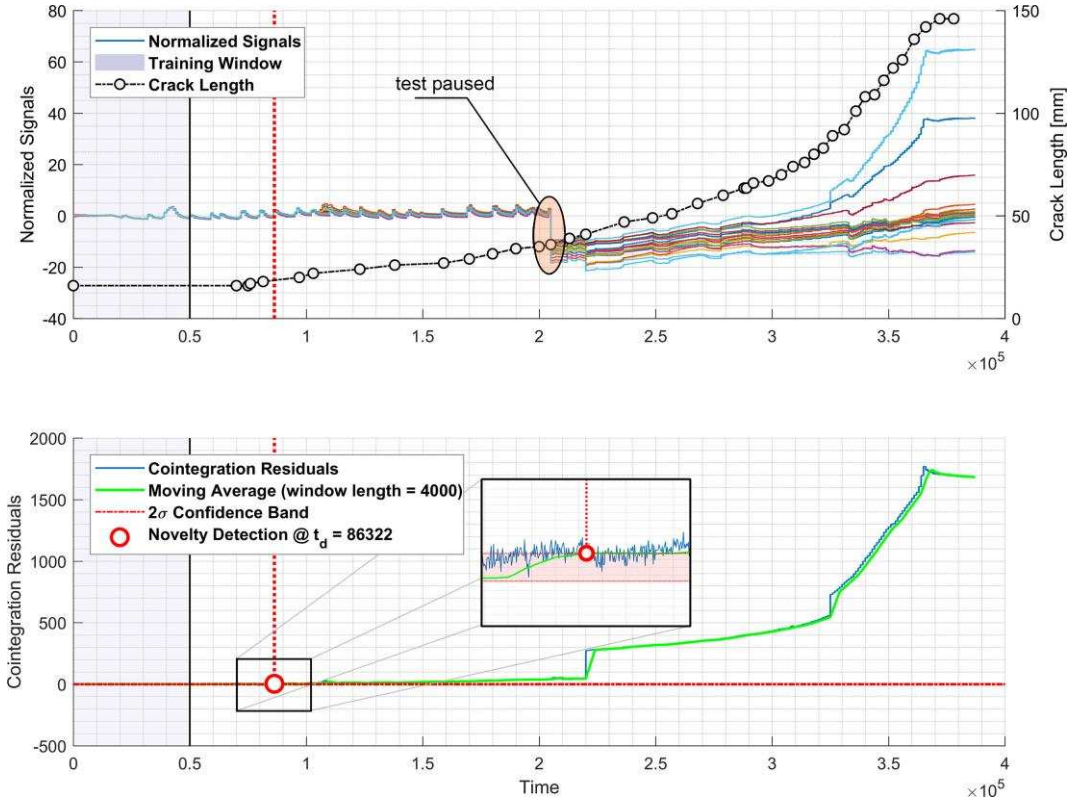

Fig. 12: Cointegration of Panel-SC test signals - all sensors are considered. In the upper plot, normalised signals (coloured) are displayed along with the crack length (black circled points) as a function of time (number of cycles). In the lower plot, the cointegration residuals are shown, with a focus of the instant when the moving average (green line) of the residuals (blue line) leaves the confidence band (in red). The training data window is highlighted in grey in both plots.

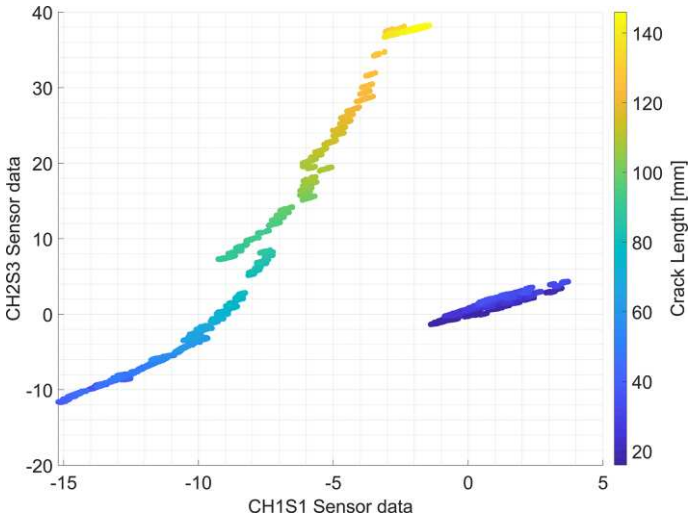

Fig. 13: Correlation plot between two signals from Panel-SC, one close to (CH2S3) and one far from (CH1S1) the crack. Colours indicate the corresponding crack length.

6.2.Fatigue crack growth detection in Panel-RC

Regarding Panel-RC, once again the detection happens fairly quickly at around 4 mm of total crack length increment as shown in Fig. 14. As anticipated in Section 3.1, three different .operational conditions. were imposed: in the second part of the experiment, the applied load is not high enough to continue crack propagation and this is reflected by the residuals, which regain their stationarity, yet remain outside the control band. When the load reaches a suitable value to restart damage growth, the residuals. absolute value increases accordingly. As previously noticed on simulated data and confirmed in Fig. 15, this highlights a correlation of the cointegration residuals with the cointegrated strain measures, and thus with the crack length, which can be further exploited in future activities for damage prognosis.

In Fig. 16a, the correlation plot, between two sensors is reported as before. A linear correlation is again present, especially in the crack-stationary portion of data (between $\times\ ^{5}$ and $\times\ ^{5}$ cycles) as Fig. 16b confirms with the group of data points in the lower left corner. Once the crack propagates further, the gradient of the linear relationship increases.

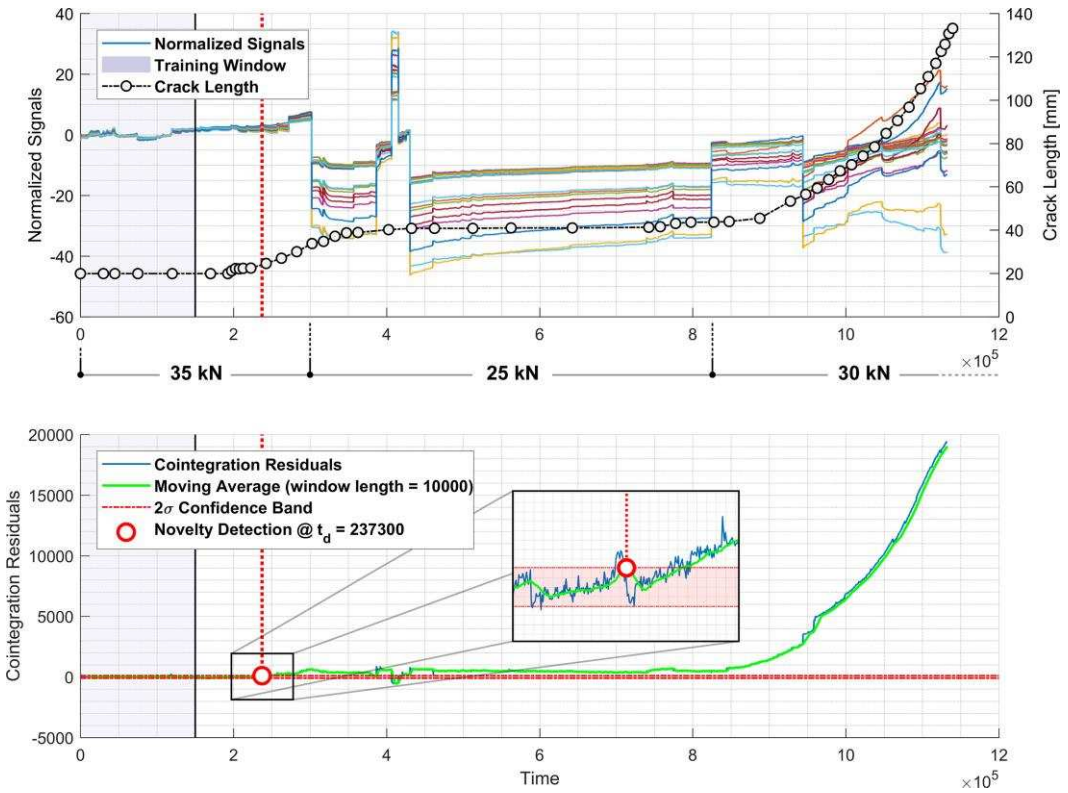

Fig. 14: Cointegration of Panel-RC test signals - all sensors are considered. In the upper plot, normalised signals (coloured) are displayed along with the crack length (black circled points) as a function of time (number of cycles). In the lower plot, the cointegration residuals are shown, with a focus of the instant when the moving average (green line) of the residuals (blue line) leaves the confidence band (in red). The training data window is highlighted in grey in both plots.

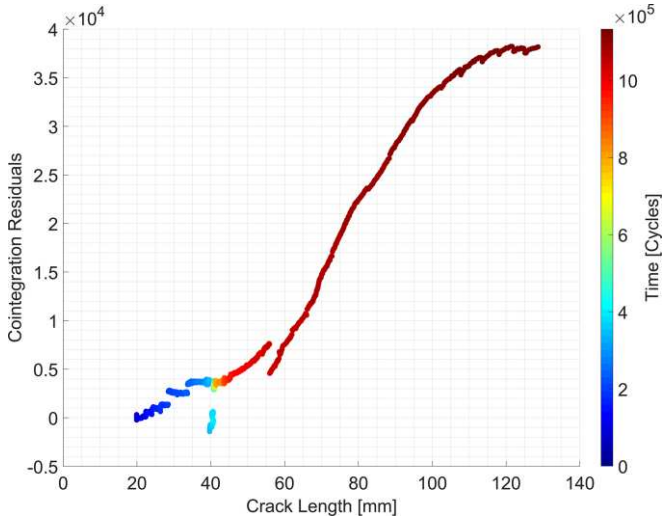

Fig. 15: Correlation plot between the cointegration residuals and the crack length trend for Panel-RC. The data points colour indicates time.

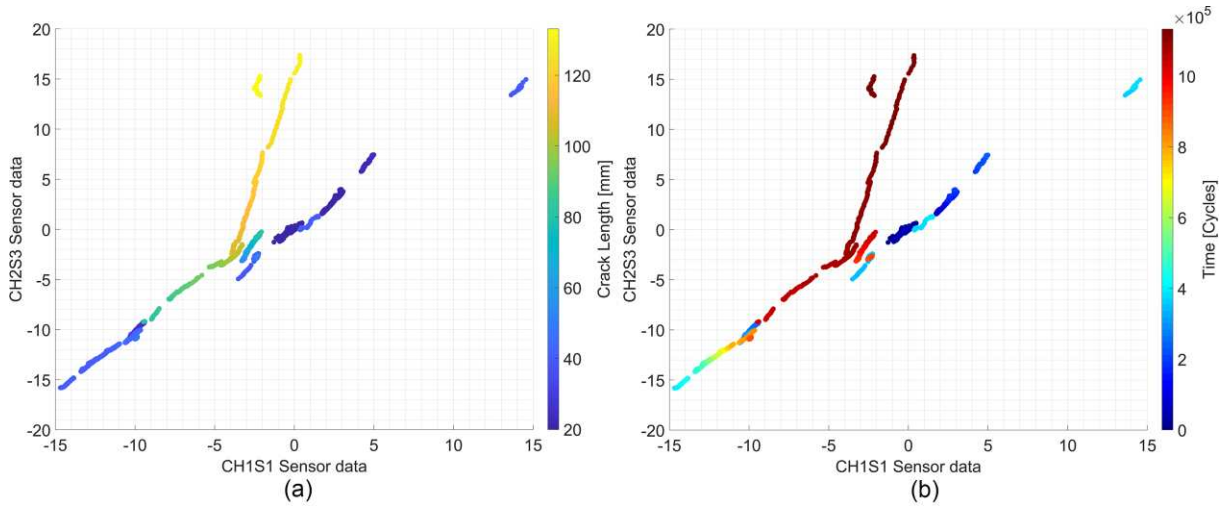

Fig. 16: Correlation plot between two signals from Panel-RC, one close to (CH2S3) and one far from (CH1S1) the crack. Colours indicate the corresponding crack length (a) and the corresponding cycle (b).

6.3.Fatigue crack growth detection in full-scale tail boom test

For the full-scale FCG test, the results are shown in Fig. 17. Once again, the initial portion of the data not affected by crack propagation is taken as the training dataset for the algorithm. Indeed, the damage was not visible during the first $\times\ ^{5}$ load cycles, so the initial data refer to the 15 mm long artificial notch. The detection is triggered at a total crack length of about 18 mm, thus equal to a 3 mm increment from the artificial notch. At around $\times\ ^{5}$ cycles, a patch was installed on the other side of the monitored tail section to prevent unwanted failures. This effect, coupled with the increasing crack propagation rate, is thought to be responsible for the second easily noticeable drift in the residuals. Again, looking at the cointegration projection of the strain signal, several discontinuities can be observed. The first kind are related to missing data from the time series: unfortunately, some cycles were not recorded properly by the acquisition system. The last kind reflects the sudden spikes in the FBG sensor signals: the behaviour of the sensors, when the sun directly hits the structure in their vicinity, is deemed not to be the same as in their normal condition. If a non-uniform strain field was applied to an FBG, its spectrum would likely become broadband [32] with the interrogator choosing a slightly different spectrum peak and following no more the original wavelength shift. Although this produces an unpredicted and transient new correlation between the different signals, manifesting as the sudden spikes of Fig. 17, the algorithm produces a usable cointegrating vector when simply coupled with a smoothing technique, in this case consisting in the moving average.

Once again, the correlation plot in Fig. 18 shows the usual stepped behaviour, with clustering of the data points related to the cycle groups between test pauses. Specifically, both the signals considered are from sensors on the same stringer, on which the crack was initiated. Gradient variation for the evolving linear relationship is less evident here mainly because the tail-boom structure is so redundant, and stiffer, that it redistributes the strain field more uniformly, coping better with a localised damage than in the panel cases.

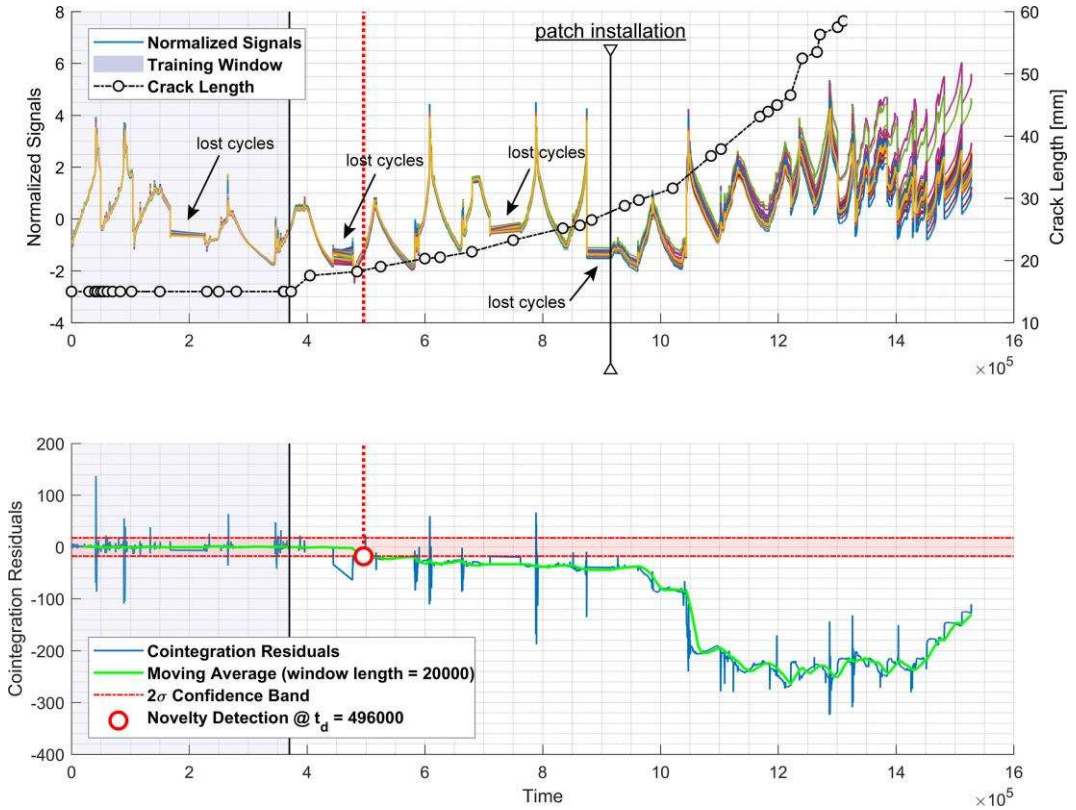

Fig. 17: Cointegration of tail boom test signals - all sensors are considered. In the upper plot, normalised signals (coloured) are displayed along with the crack length (black circled points) as a function of time (number of cycles). In the lower plot, the cointegration residuals are shown, with a focus of the instant when the moving average (green line) of the residuals (blue line) leaves the confidence band (in red). The training data window is highlighted in grey in both plots.

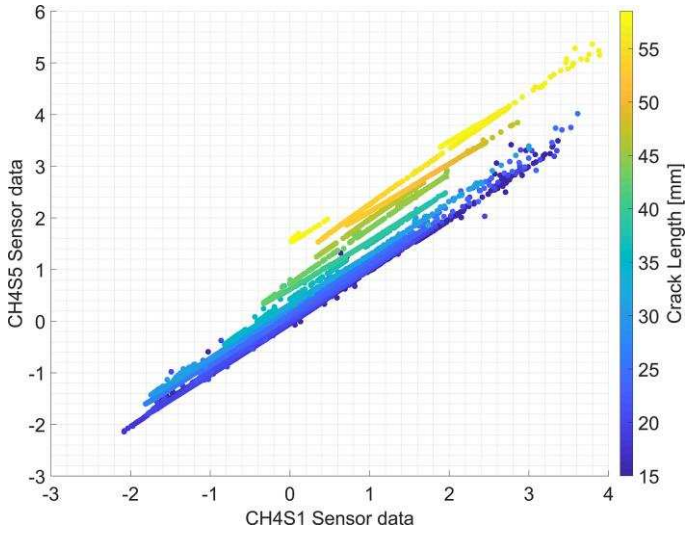

Fig. 18: Correlation plot between two signals from the tail boom, one close to (CH4S5) and one far from (CH4S1) the crack. Colours indicate the corresponding crack length.

Finally, the sensitivity of the method towards the distance of the sensors from the damage location is illustrated in Fig. 19. Specifically, only sensors on stringer number 7, which is the one where the crack propagated, are taken into account and their cointegration relationship is analysed in pairs. Such a performance is in reasonable agreement with the current damage tolerance regulation indicated in [33], in both cases when the entire sensor network is taken into account and when just only the two sensors on the

stringer closest to the damage are considered. The algorithm results are shown in terms of crack length at detection time for different sensor pairs, compared to the detection time obtained including all the sensors into the cointegration procedure. As expected intuitively, the farther the selected sensors are from the damage location, the later the anomaly is revealed by a residual drift out of the control interval. If all sensors are considered, the algorithm performances are comparable with the case of the sensors S5-S6. Further investigations, which however fall outside the scope of the present study, should be carried on in this direction to assess the existence of an optimal number of sensors considered, although this could strongly depend on the characteristics of the specific analysed case.

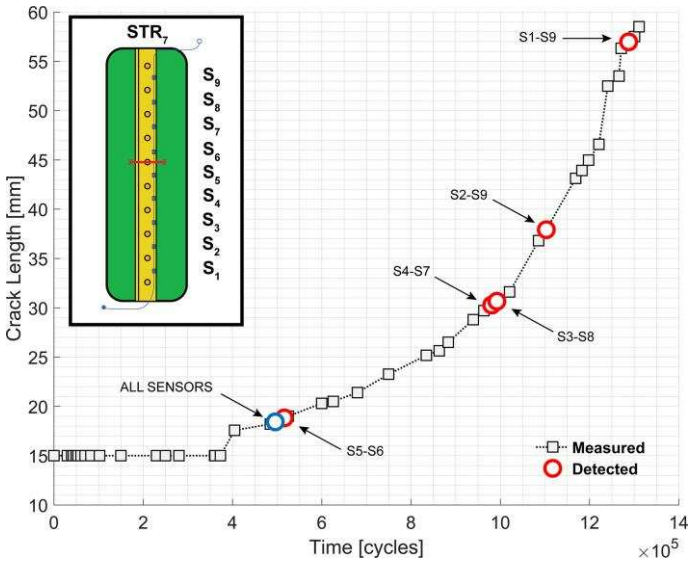

Fig. 19: Anomaly detection using different sensor pairs on stringer STR7 with the rivet crack.

7. Conclusions

In the present study, the cointegration-based signal processing method presented in [5,19] has been applied to strain signals recorded through FBG sensor networks for fatigue crack detection on aeronautical structures. Both numerically-simulated data and signals collected in a laboratory environment were used to investigate the algorithm performance.

The numerical simulation activity has been conducted with the aim of exploring the effectiveness of the method in the context of fatigue crack growth and to assess its sensitivity to the size of training dataset, specifically including increasing crack lengths into the training set. Looking at the correlation between two sensors during damage evolution, it is clear that they initially exhibit a linear correlation, with a gradient generally increasing with crack propagation, finally exhibiting a non-linear correlation at very high damage extents. As a consequence, even if the training dataset contains some information about initial linear correlations, residual deviation from the normal condition is guaranteed by the subsequent gradient increase and by the final degeneration into non-linear correlation.

Once the method.s capabilities have been proven for damage detection, the same approach has been employed to remove the undesired trend from the experimental data. Indeed, cointegration has been shown to be an effective temperature compensation technique for FBG sensor signals. The raw sensor outputs can be directly used and projected on the calculated cointegrating vector without caring for an otherwise needed compensation coefficient optimisation and one or more dedicated temperature transducers.

Regarding performance, among the three different FCG tests, the applied method has been capable of detecting the onset of damage propagation within a 4 mm increment from the baseline condition. This result has been achieved even in the presence of large temperature fluctuations hiding the very small crack-induced strain variations, as in the full-scale fatigue test conducted on a helicopter tail boom. Thus, with cointegration, compensation of environmental changes that repeatedly appear during the system operation and anomaly detection can be accomplished in one-step and without any additional post-processing algorithm.

As it was preliminarily done based on simulations, the experimental cointegration residuals are always interpreted by analysing the evolution of the correlation between two test sensors, nevertheless considering that this does not provide a complete picture of the behaviour of the residuals. It was further noticed that the cointegration residuals correlates well with damage extent, as shown with simulations and in a test with variable amplitude fatigue load and consequent discontinuous damage trends, thus potentially leading to future exploitation of the method in the context of damage prognosis.

Finally, a qualitative indication has been provided about the sensitivity of the method towards the distance of the considered sensors from the damage location: the closer the sensor is, the better the damage detection performance.

The foreseen drawbacks of the method, however, consist primarily in the linear correlation required for the time series in order to apply the Johansen procedure. Then, focusing on the specific applications of the present paper, the choice of strain load peaks as reference features for damage identification may not be appropriate in cases when the fatigue load applied on the structure has a random spectrum. Indeed, the strain peaks would change randomly (with the exception of changes in the operational conditions) and the signals would be already stationary and not integrated of order one, which is one of the main assumptions for cointegration to work. Therefore, the use of such a feature is questionable in real cases where the structure is subjected to random loads, and the use of other more robust features should be investigated. Having noted this, the strain peak time series could still be of use in cases where transient overloads need to be monitored over a cyclic load conditions (such as manufacturing processes and rotating machinery in general). Furthermore, the ideas presented in this study are directed towards an offline approach where the baseline signals are defined and unchanged during time, while an online version of the method, able to discriminate autonomously between different operational conditions or relying on features insensitive to the boundary load, would be of more practical value.

Nevertheless, the present application confirms the potential of cointegration presented in previous works for case studies concerning laboratory scenarios or civil structures. Specifically, the method has proven its effectiveness also at detecting growing and propagating cracks in real structures and not only sudden damages or transient anomalous behaviour.

Acknowledgements

This work has been developed based on the results from ASTYANAX project (Aircraft fuSelage crack monitoring sYstem And progNosis through on-boArd eXpert sensor network), a Cat.-B project coordinated by the European Defense Agency (EDA) and involving three nations: Italy (Politecnico di Milano, AleniaAermacchi, AgustaWestland), Poland (Instytut Techniczny Wojsk Lotniczych - AFIT, Military Aviation Works No. 1, AGH University of Science and Technology) and Spain (Instituto Nacional de Técnica Aeroespacial - INTA). Keith Worden gratefully thanks the UK Engineering and Physical Sciences Research Council for funding his Established Career Fellowship.

References

[1] C.R. Farrar, K. Worden, Structural Health Monitoring: A Machine Learning Perspective, John Wiley & Sons, Ltd, Chichester, UK, 2012. doi:10.1002/9781118443118.

[2] E.J. Cross, K.Y. Koo, J.M.W. Brownjohn, K. Worden, Long-term monitoring and data analysis of the Tamar Bridge, Mechanical Systems and Signal Processing. 35 (2013) 16–34. doi:10.1016/j.ymssp.2012.08.026.
[3] H. Sohn, Effects of environmental and operational variability on structural health monitoring, Philosophical Transactions of the Royal Society A: Mathematical, Physical and Engineering Sciences. 365 (2007) 539–560. doi:10.1098/rsta.2006.1935.
[4] K. Worden, T. Baldacchino, J. Rowson, E.J. Cross, Some Recent Developments in SHM Based on Nonstationary Time Series Analysis, Proceedings of the IEEE. (2016) 1–15. doi:10.1109/JPROC.2016.2573596.
[5] E.J. Cross, K. Worden, Q. Chen, Cointegration: a novel approach for the removal of environmental trends in structural health monitoring data, Proceedings of the Royal Society A: Mathematical, Physical and Engineering Sciences. 467 (2011) 2712–2732. doi:10.1098/rspa.2011.0023.
[6] E.J. Cross, G. Manson, K. Worden, S.G. Pierce, Features for damage detection with insensitivity to environmental and operational variations, Proceedings of the Royal Society A: Mathematical, Physical and Engineering Sciences. 468 (2012) 4098–4122. doi:10.1098/rspa.2012.0031.
[7] P.B. Dao, W.J. Staszewski, Data normalisation for Lamb wave–based damage detection using cointegration: A case study with single- and multiple-temperature trends, Journal of Intelligent Material Systems and Structures. 25 (2014) 845–857. doi:10.1177/1045389X13512186.
[8] P.B. Dao, W.J. Staszewski, Cointegration approach for temperature effect compensation in Lamb-wave-based damage detection, Smart Materials and Structures. 22 (2013) 095002. doi:10.1088/0964-1726/22/9/095002.
[9] E.J. Cross, K. Worden, Approaches to nonlinear cointegration with a view towards applications in SHM, Journal of Physics: Conference Series. 305 (2011) 012069. doi:10.1088/1742-6596/305/1/012069.
[10] H. Shi, K. Worden, E.J. Cross, A nonlinear cointegration approach with applications to structural health monitoring, Journal of Physics: Conference Series. 744 (2016) 012025. doi:10.1088/1742-6596/744/1/012025.
[11] K. Worden, E.J. Cross, I. Antoniadou, A. Kyprianou, A multiresolution approach to cointegration for enhanced SHM of structures under varying conditions – An exploratory study, Mechanical Systems and Signal Processing. 47 (2014) 243–262. doi:10.1016/j.ymssp.2013.10.012.
[12] A.A. Tabrizi, H. Al-Bugharbee, I. Trendafilova, L. Garibaldi, A cointegration-based monitoring method for rolling bearings working in time-varying operational conditions, Meccanica. 52 (2017) 1201–1217. doi:10.1007/s11012-016-0451-x.
[13] H. Zhao, H. Liu, H. Ren, H. Liu, The condition monitoring of wind turbine gearbox based on cointegration, in: IEEE, 2016: pp. 1–6. doi:10.1109/POWERCON.2016.7753906.
[14] M. Corbetta, C. Sbarufatti, E.J. Cross, M. Giglio, Removal of temperature-induced strain variations for fatigue crack growth detection in a real aeronautical structure, in: 2016: p. 10.
[15] M. Kreuzer, Strain Measurement with Fiber Bragg Grating Sensors, 2006.
[16] B.J. Soller, T.C. Haber, A. Mendez, Temperature Effects and Fiber Optics Sensors in Structural Health Monitoring Applications, in: The ISHMII Monitor, 2013.
[17] A.-M. Yan, G. Kerschen, P. De Boe, J.-C. Golinval. Structural damage diagnosis under varying environmental conditions - Part I: A linear analysis. Mechanical Systems and Signal Processing 19, 2005;847:864.
[18] A.-M. Yan, G. Kerschen, P. De Boe, J.-C. Golinval. Structural damage diagnosis under varying environmental conditions - Part II: local PCA for non-linear cases. Mechanical Systems and Signal Processing 19, 2005;865:880.
[19] E.J. Cross, K. Worden, Cointegration and why it works for SHM, Journal of Physics: Conference Series. 382 (2012) 012046. doi:10.1088/1742-6596/382/1/012046.
[20] B.C. Lee, G. Manson, W.J. Staszewski, Environmental Effects on Lamb Wave Responses from Piezoceramic Sensors, Materials Science Forum. 440–441 (2003) 195–202. doi:10.4028/www.scientific.net/MSF.440-441.195.
[21] Y. Liang, D. Li, G. Song, Q. Feng, Frequency Co-integration-based damage detection for bridges under the influence of environmental temperature variation, Measurement. 125 (2018) 163–175. doi:10.1016/j.measurement.2018.04.034.
[22] P.B. Dao, A. Klepka, Ł. Pieczonka, F. Aymerich, W.J. Staszewski, Impact damage detection in smart composites using nonlinear acoustics cointegration analysis for removal of undesired load effect, Smart Materials and Structures. 26 (2017) 035012. doi:10.1088/1361-665X/aa5744.
[23] T.W. Anderson, The Statistical Analysis of Time Series, Wiley, 2011. https://books.google.it/books?id=rCOzXIC8ZLkC.
[24] R. Perman, Cointegration: An Introduction to the Literature, Journal of Economic Studies. 18 (1991). doi:10.1108/EUM0000000000151.
[25] D.A. Dickey, W.A. Fuller, Distribution of the Estimators for Autoregressive Time Series With a Unit Root, Journal of the American Statistical Association. 74 (1979) 427. doi:10.2307/2286348.
[26] D.A. Dickey, W.A. Fuller, Likelihood Ratio Statistics for Autoregressive Time Series with a Unit Root, Econometrica. 49 (1981) 1057. doi:10.2307/1912517.
[27] W.A. Fuller, Introduction to statistical time series, 2. ed, Wiley, New York, 1996.
[28] S. Johansen, Likelihood-based inference in cointegrated vector autoregressive models, Reprinted, Oxford Univ. Press, Oxford, 2009.
[29] N.E. Dowling, K.S. Prasad, R. Narayanasamy, Mechanical Behavior of Materials: Engineering Methods for Deformation, Fracture, and Fatigue, Pearson, 2013. https://books.google.it/books?id=OrlxMAEACAAJ.
[30] C.C.J. Poe, Stress-intensity factor for a cracked sheet with riveted and uniformly spaced stringers, NASA, 1971.
[31] D. Montgomery, Introduction to statistical quality control, 2009. doi:10.1002/qre.4680070316.
[32] H. Ling, K. Lau, L. Cheng, K. Chow, Embedded fibre Bragg grating sensors for non-uniform strain sensing in composite structures, Measurement Science and Technology. 16 (2005) 2415–2424. doi:10.1088/0957-0233/16/12/003.
[33] Joint Service Specification Guide, Aircraft Structures, Department of Defense, 2006.

Figure Captions

Fig. 1: Experimental test configuration for the aeronautical panels, on the left, and location of FBG sensors and cracks (rivet crack, RC, and skin crack, SC) on the right.

Fig. 2: Experimental test configuration of the Mi-8 helicopter tail boom (a) and location of the crack monitored during the FCG tests.

Fig. 3: Example of the acquired FBG signals with highlighted peaks (a) and variation of mean value of the strain peaks (b) due to temperature shift (black dash-dot line, measured by the dedicated FBG sensor).

Fig. 4: FEM model (right) with highlighted components and Panel-RC with superimposed stress contour plot.

Fig. 5: Strain values (E22 component, vertical direction) of the 20 simulated sensors for the case without (a) and with (b) thermal field.

Fig. 6: Simulated strain signals and crack length history (a) and temperature signal from the compensator sensor (resampled and smoothed).

Fig. 7: Simulated strain signals at a constant 35kN reference load, with superimposed temperature effect, and crack length history.

Fig. 8: Cointegration of FEM signals - all sensors are considered. In the upper plot, normalised signals (coloured) are displayed along with the crack length (black circled points) as a function of time (number of cycles). In the lower plot, the cointegration residuals are shown, with a focus of the

instant when the moving average (green line) of the residuals (blue line) leaves the confidence band (in red). The training data window is highlighted in grey in both plots.

Fig. 9: Correlation plot between two of the FEM-generated signals, one from a virtual sensor close to the crack (CH2S3) and one relatively away from it (CH1S1). The different data points are coloured accordingly to the corresponding semi-crack length value.

Fig. 10: Detection time and crack length at detection as a function of number of cycles considered as training data (a) and as a function of the crack length at the end of the considered training data (b).

Fig. 11: Correlation plot between the cointegration residuals and the crack length trend for the simulated panel case. The data points colour indicates time.

Fig. 12: Cointegration of Panel-SC test signals - all sensors are considered. In the upper plot, normalised signals (coloured) are displayed along with the crack length (black circled points) as a function of time (number of cycles). In the lower plot, the cointegration residuals are shown, with a focus of the instant when the moving average (green line) of the residuals (blue line) leaves the confidence band (in red). The training data window is highlighted in grey in both plots.

Fig. 13: Correlation plot between two signals from Panel-SC, one close to (CH2S3) and one far from (CH1S1) the crack. Colours indicate the corresponding crack length.

Fig. 14: Cointegration of Panel-RC test signals - all sensors are considered. In the upper plot, normalised signals (coloured) are displayed along with the crack length (black circled points) as a function of time (number of cycles). In the lower plot, the cointegration residuals are shown, with a focus of the instant when the moving average (green line) of the residuals (blue line) leaves the confidence band (in red). The training data window is highlighted in grey in both plots.

Fig. 15: Correlation plot between the cointegration residuals and the crack length trend for Panel-RC. The data points colour indicates time.

Fig. 16: Correlation plot between two signals from Panel-RC, one close to (CH2S3) and one far from (CH1S1) the crack. Colours indicate the corresponding crack length (a) and the corresponding cycle (b).

Fig. 17: Cointegration of tail boom test signals - all sensors are considered. In the upper plot, normalised signals (coloured) are displayed along with the crack length (black circled points) as a function of time (number of cycles). In the lower plot, the cointegration residuals are shown, with a focus of the instant when the moving average (green line) of the residuals (blue line) leaves the confidence band (in red). The training data window is highlighted in grey in both plots.

Fig. 18: Correlation plot between two signals from the tail boom, one close to (CH4S5) and one far from (CH4S1) the crack. Colours indicate the corresponding crack length.

Fig. 19: Anomaly detection using different sensor pairs on stringer STR7 with the rivet crack.